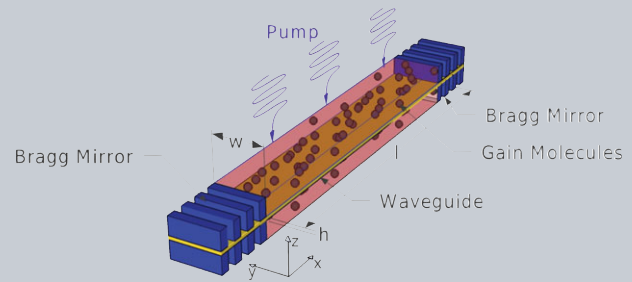


**Abstract** It is shown that lasing action at subwavelength scales can be achieved in realistic plasmonic systems supporting long-range surface plasmons (LRSPs). To this end, a general numerical framework has been developed that is able to accurately account for the full spatio-temporal lasing dynamics and the vastly different length- and time-scales featured by this class of systems. Starting from a loss compensation regime for propagating LRSPs, it is shown how the introduction of an optical feedback mechanism induces the formation of a self-sustained laser oscillation at moderate pump intensities. The simplicity of the proposed subwavelength scale laser offers significant potential as a novel class of planar light sources in complex plasmonic circuits.



## Lasing action assisted by long-range surface plasmons

Felix Rütting, Javier Cuerda, Jorge Bravo-Abad, and Francisco J. Garcia-Vidal\*

Long-range surface plasmons (LRSPs) are optical surface modes supported by symmetric insulator-metal-insulator structures [1]. The unique properties featured by these modes have drawn significant interest, both from fundamental and applied points of view. As already indicated by their name, the propagation losses of LRSPs are very small compared to other plasmonic modes. This fact, together with their ability for confining light at subwavelength scales in the transversal direction, has made LRSPs promising platforms for the development of a number of planar photonic components [2, 3].

On a different note, a number of recent works have successfully demonstrated the feasibility of achieving nanoscale lasing action assisted by a variety of plasmonic resonances. In general, these plasmonic lasers can be classified by the nature of the considered surface plasmon resonance. Plasmonic lasing action can be based on localized plasmonic surface modes [4–9], or, alternatively, on propagating surface plasmons [10–12]. Of special interest in this last category is the recent realization of a plasmonic laser assisted by deep-subwavelength propagating gap plasmons supported by hybrid deep-subwavelength plasmonic waveguides [10, 12]. While lasing action in systems based on localized plasmons requires compensation of the losses, for the those based on propagating plasmons loss compensation and a feedback mechanism is needed. An alternative to those two routes are lasers that employ stopped-light [13], as they enable lasing action without cavities and without threshold.

Very recently Kéna-Cohen *et al.* [14] have successfully demonstrated confined plasmonic amplifiers based on LRSPs. The extension of these findings to the development of LRSPs subwavelength scale lasers would represent an important advance in the field of subwavelength coherent

light sources. The potential of LRSPs for plasmonic amplifiers and lasers is significant due to the following reasons. First, the low propagation losses featured by LRSPs reduce the optical gain required for full-loss compensation, and, therefore, bring closer the prospect of reaching the lasing onset at moderate pump powers. Second, the rate of spontaneous emission of a dipolar emitter into LRSPs is remarkably low [14, 15]. This enables low-noise optical amplification and, due to the well-defined TM polarization of LRSP modes, laser action with low polarization noise [15]. Of course, the low coupling to spontaneous emission also yields an increase of the lasing threshold via the effective reduction of the corresponding  $\beta$ -factor. Finally, by taking advantage of the all previous technology developed for creating on-chip LRSP components, LRSP lasers are suitable for their integration in complex optical circuits.

In this Letter, we theoretically demonstrate that lasing action can be achieved in realistic LRSP geometries, and we present an extensive study of the lasing action of this class of subwavelength scale lasers. For this purpose, we have developed a complete general numerical framework, which allows tracking accurately the spatio-temporal evolution of the relevant physical magnitudes governing the lasing action in the considered systems. Using this general formalism, we go beyond the ohmic-loss compensation regime and show that, for moderate values of the pump power, self-sustained laser oscillations can be observed in LRSP structures that include an optical feedback mechanism.

Figure 1 renders a sketch of a possible realization of the considered LRSP lasers. A thin metallic waveguide is embedded within two layers of gain material and the whole structure is enclosed in an homogeneous dielectric medium with a refractive index of  $n = 1.71$ . We assume that the

Departamento de Física Teórica de la Materia Condensada and Condensed Matter Physics Center (IFIMAC), Universidad Autónoma de Madrid, E-28049, Spain

\*Corresponding author(s): e-mail: fj.garcia@uam.es

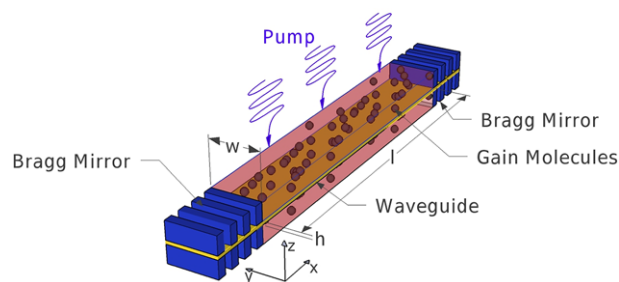


**Figure 1** Sketch of the considered lasing device based on LR-SPPs. The optical gain is provided by organic molecules below and above the waveguide, while optical feedback is created by the Bragg mirrors located at the ends of the waveguide.

optical feedback needed for reaching the lasing onset is introduced by including a reflection mechanism at the ends of the waveguide. These reflective waveguide boundaries can be realized with Bragg mirrors designed to display a large reflection coefficient for the LRSPS propagating along the structure [16]. The simulation of lasing action in these devices requires a numerical method capable of accounting for the full spatio-temporal dynamics that results from the interplay between the highly non-uniform electromagnetic field supported by the structure and the electronic dynamics of the molecules that form the gain medium. This is a particularly challenging problem due to the vastly different temporal and spatial scales involved in the problem. On one hand, the smallest length scale in the considered LRSPS laser geometry is given by the height  $h$  of the waveguide. Following the recent experiment [14], a value of  $h = 21$  nm is assumed in all the calculations displayed in this work. On the other hand, the largest length scale in the problem is set by the length  $l$  of the LRSPS waveguide, in our case  $l$  is of the order of a few microns. As shown below the minimum length required for reaching the lasing regime depends on the effective gain and the reflectivity of the boundaries. Regarding the different time-scales involved in this problem, the minimum time scale is set by the fast femtosecond optical oscillation of the electromagnetic fields, whereas the maximum time-scale is defined by the slowest electronic decays of the considered molecular states, which are of the order of a few nanoseconds.

In order to tackle this challenging numerical problem, we have generalized a recently proposed finite element method (FEM) approach for simulating active structures [17] to three-dimensional lasing systems with reflective boundaries. The adaptive mesh featured by this FEM approach allows the efficient discretization of all geometrical characteristics of the considered systems. Before proceeding, we present an overview of the numerical method developed in this work (a detailed description can be found in the Supporting Information). As in the experimental realization of the LRSPS amplifier [14], organic molecules (DCM molecules) dispersed in a host medium ( $Alq_3$ ) are used as gain medium in our simulations. This allows us to fit all free parameters of our gain dynamics model to the experimental results. In order to pro-

vide gain in this system, the host is optically pumped and the energy is transferred via Förster energy transfer to the DCM-molecules. In contrast to the also widely used dye-molecules [18–20], gain saturation in this guest-host system is not mainly reached by excitation of all DCM-molecules, but rather the gain is limited by a bimolecular annihilation mechanism. This bimolecular annihilation also limits the influence of the Purcell-effect at high pump intensities, as illustrated later on in the discussion of the propagation properties of LRSPS in these waveguides.

A simple set of rate equations governing the dynamics of the populations, which includes bimolecular annihilation, is given by:

$$\partial_t N_{Alq} = G - \frac{N_{Alq}}{\tau_{Alq}} - k_t N_{Alq} \quad (1)$$

$$\begin{aligned} \partial_t N_{DCM} = & k_t N_{Alq} - \frac{N_{DCM}}{\tau_{DCM}} - k_{an} N_{Alq} N_{DCM} \\ & + \frac{1}{2\hbar\omega} \text{Re} \left( \partial_t \vec{P} \cdot \vec{E}^* \right). \end{aligned} \quad (2)$$

Here  $N_{Alq}$  and  $N_{DCM}$  are the densities of excited  $Alq$ - and  $DCM$ -molecules, respectively.  $G$  is the pump rate,  $\tau_{Alq}$  and  $\tau_{DCM}$  are the corresponding molecular lifetimes,  $k_t$  is the Förster transfer rate (which depends on  $N_{DCM}$  and on the total density of DCM-molecules  $N_0 = 3 \cdot 10^{19} \text{ cm}^{-3}$ ), and  $k_{an}$  is the  $Alq$ - $DCM$ -annihilation rate. The numerical values of all constants are given in the Supporting Information. The polarization density  $\vec{P}$  depends on both the electromagnetic field and the density of excited DCM molecules. Therefore,  $\vec{P}$  is the key magnitude that couples the molecular dynamics to the EM field. In Eq. (2), the stimulated emission term is averaged over one period of the emission frequency  $\omega$  of the DCM molecules.

In our simulations, the gain medium is pumped at a wavelength of  $\lambda_{pump} = 355$  nm, while the emission wavelength of the organic molecules is  $\lambda = 633$  nm. This significant spectral separation of the pump field and the LRSPS (which in turn will be located close to the emission wavelength) allows to solve the field equations for the pump and for the plasmon separately. In our approach we introduce an approximation based on treating the two contributions separately. The validity of this approximation is guaranteed by the large spectral separation between both contributions. Splitting all electromagnetic fields in a part related to the pump and a second one related to the LRSPS allows to use an ansatz suitable for the time dynamics of the systems under continuous-wave pumping. Specifically, in terms of the magnetic potential vector  $\vec{A}(t)$ , this ansatz can be expressed as

$$\vec{A}(t) = \vec{A}(t) e^{-i\omega t}. \quad (3)$$

As the fast dynamic related to the optical frequency  $\omega$  is included in the harmonic factor in Eq. (3),  $\vec{A}$  only varies slowly on time scales defined by the dynamics of the

molecules. Using a similar ansatz for all fields allows to speed-up the simulation significantly without using any approximation. It should be noticed that the main approximation introduced in this approach is not the use of the ansatz given in Eq. (3), which is only a reformulation of the time dependency, but rather the splitting of the field in two parts. This splitting is essential for the practical application of the used ansatz. This, in turn, allows us to study the dynamics of the system up to the nanosecond time-scale. Notice also that the splitting of the field equations in two parts does not affect the fact that the dynamics of the LRSPP is coupled to the pump field via the electronic rate-equations characterizing the gain medium.

The conventional formulation for time-dependent simulations of electromagnetic fields consists in expressing the field dynamics with the help of the vector potential  $\vec{A}$  [21], so that the field equation reads

$$\nabla \times \left[ \frac{1}{\mu_0} \nabla \times \vec{A} \right] + \epsilon_r \epsilon_0 \partial_t^2 \vec{A} = \partial_t \vec{P}. \quad (4)$$

In Eq. (4),  $\epsilon_r$  is the time-independent part of the relative permittivity, while the time-dependent part is included in  $\vec{P}$ . In the numerical approach introduced in this work, the above equation is solved using the so-called *weak-form* formulation [21]. This approach consists, first, in multiplying Eq. (4) by a test-function and, then, integrating the resulting product over the whole simulation domain. As explained in detail in the Supporting Information, a boundary term appears after performing a partial integration. This boundary term can be used to obtain the solution with the desired physical boundary conditions. In the case of reflective boundaries (required for the simulation of LRSPP lasers) the knowledge of the spatial profile of the mode which should be reflected is needed. In our implementation, we obtain that spatial profile from simulations of a LRSPP propagating in a passive waveguide without organic molecules. In this way, the reflectivity of the boundaries is adapted to the passive system, as it would be in an experimental realization. Finally, noise and spontaneous emission [19] are not accounted for in the presented study. As LRSPP are known to couple only very weakly to spontaneous emission [14, 15], noise is expected to be a minor effect in our system.

As a first step towards plasmonic lasing enabled by long-range surface plasmons, we discuss the propagation properties of LRSPPs in the considered structure. These properties provide the basis for understanding the lasing behavior and allow us to fit the parameters of our microscopic model of the organic molecules to available experimental results [14]. The solid lines in Fig. 2 show the dependency of the imaginary part of the propagation constant of the LRSPP on the pump intensity for a gold-based waveguide. The geometrical parameters in this simulation are the same as those by Kéna-Cohen *et al.* [14]. As mentioned above, the waveguide height is  $h = 21$  nm. The width of the waveguide  $w$  is chosen to be  $w = 1 \mu\text{m}$ . On top of the waveguide we place a 130 nm-thick layer of organic molecules. We

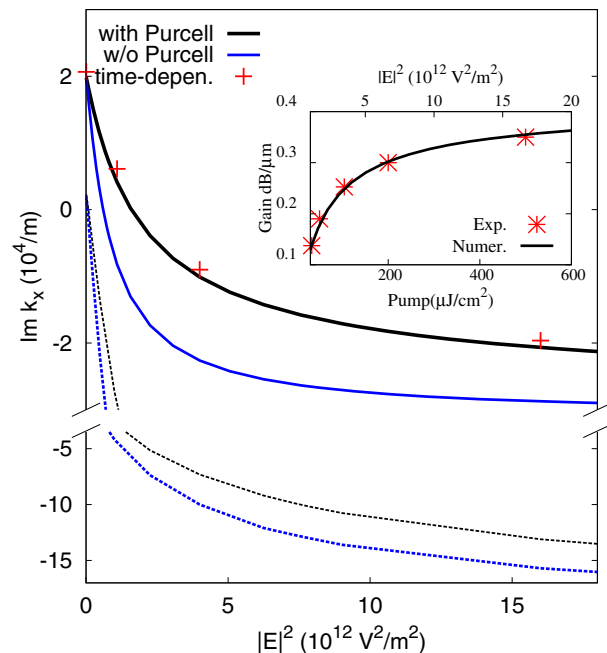


**Figure 2** Propagation properties. The solid lines show the dependency of the imaginary part of the propagation constant on the pump intensity for a  $1 \mu\text{m}$ -wide and  $21 \text{ nm}$ -high gold waveguide with a  $130 \text{ nm}$  high layer of organic molecules on top. As shown by the decreasing separation of the blue (without) and black (with) line, the Purcell effect becomes less influential for higher pumps, as bimolecular annihilation increases. The inset shows the agreement of the numerical results for used parameter with the experimental results of Kéna-Cohen *et al.* [14] (experimental results are taken from Fig. 3 within the reference). The dashed lines show the propagation properties of the modified system used in lasing simulations.

assume that these molecules are optically pumped from above. As clearly observed in Fig. 2, full-loss compensation and amplification ( $\text{Im}(k_x) < 0$ ) can be reached, and for the highest pump intensities  $\text{Im}(k_x)$  saturates at values in the order of  $-2 \times 10^4 \text{ m}^{-1}$ .

The comparison of the results with and without Purcell effect (black and blue lines, respectively, in Fig. 2) illustrates the influence of the Purcell effect on the effective gain. For the smaller intensities of the pump field ( $|E_{\text{pump}}|^2 < 5 \cdot 10^{12} \text{ V}^2/\text{m}^2$ ), the reduced lifetime of the excited DCM state results in a significantly reduced gain coefficient when the Purcell effect is included. This effect is less pronounced for larger values of  $E_{\text{pump}}$ , mainly due to the fact that the bimolecular annihilation becomes significant at higher density of excited molecules.

For a waveguide without feedback, the intensity of the LRSPP is much smaller than the pump field. Therefore, the depopulation of the excited DCM state due to stimulated emission can be neglected. This fact allows us to carry out an alternative calculation of the propagation properties of the considered active systems by applying the following time-independent approach. First, we compute the spatial field distribution of the pump field  $\vec{E}_{\text{pump}}(\vec{r})$ . Then, we

calculate the pump rate  $G(\vec{r})$  at each point within the gain layer by using

$$G(\vec{r}) = \frac{1}{2\omega_{pump}\hbar} c\epsilon_0\alpha n_{host} |\vec{E}_{pump}(\vec{r})|^2, \quad (5)$$

where  $\omega_{pump}$  is the pump frequency,  $\alpha$  is the absorption coefficient and  $n_{host}$  is the refractive index of the host. After that, we use the fact that, for a given time-independent pump rate, the set of electronic rate equations given by Eqs. (1) and (2) has a steady solution when neglecting the last term on the right-hand side of Eq. (2). This approximation is justified because the neglected term is precisely the one that describes stimulated emission processes. The resulting population density  $N_{DCM}(\vec{r})$  is employed to find the spatial distribution of the relative permittivity  $\epsilon_r(\vec{r})$  at the wavelength of the LRSPP. Finally, we use the resulting  $\epsilon_r(\vec{r})$  to compute, via an eigenmode calculation, the corresponding propagation constant of the LRSPPs.

The results from these simulations are summarized in Fig. 2. Solid lines in this figure render the results obtained via eigenmode-calculations, while the red crosses display our results for the corresponding steady-state values as obtained from time-dependent calculations. The good agreement between the time-dependent calculations and the eigenmode-calculations illustrates that, indeed, stimulated emission can be neglected for propagating LRSPP. The small differences between the results are mainly due to different discretization meshes used in both types of calculations.

Lasing action in devices based on propagating surface plasmons requires of both effective gain and an optical feedback mechanism. The above discussion on the propagation properties shows that effective gain can indeed be achieved in the considered class of systems under realistic conditions. Thus, in order to access the lasing regime, a feedback mechanism must be implemented on the considered structure. In this work, this feedback mechanism is added by assuming that the boundaries of the waveguide have a certain reflectivity, described by a reflection coefficient  $r$ . Experimentally, reflective boundaries for LRSPP have been realized as Bragg mirrors [16]. The required absolute value of  $r$  is determined by the effective gain and the length of the waveguide  $l$ . This dependence simply reflects the fact that lasing can only be achieved if all loss channels in the system are fully compensated. Mathematically, the condition for lasing can be formulated as  $r \exp[-\text{Im}(k_x)l] \geq 1$ . Due to the complexity of the simulations, only waveguides with a length of a few microns are numerical accessible. Considering that the propagation constant is limited to values of  $\text{Im}(k_x) \gtrsim -2 \cdot 10^4 \text{ m}^{-1}$  (see Fig. 2), the requirement for full-loss compensation indicates that lasing can be only expected for boundaries with a very large reflection coefficient  $r > 0.98$ . However, it should be highlighted that this restriction to very high reflectivities only stems from numerical limitations. In experimental realizations, active systems based on LRSPP waveguides with lengths of up to  $40 \mu\text{m}$  have been demonstrated [14]. For waveguides of that

length, the condition of full-loss compensation is fulfilled for values of the reflection coefficient  $r > 0.44$ .

In the Supporting Information we show that a simplified two-dimensional model can be used for simulating lasing action in a very long waveguide ( $l \approx 40 \mu\text{m}$ ). However, for the purpose of reaching the lasing regime within the full three-dimensional simulation, in the rest of this letter we modify the system in order to allow for a higher effective gain. Specifically, we introduce the following changes. First, a second layer of organic molecules is added below the waveguide, in order to take advantage of the symmetry of the LRSPP with respect to the waveguide. Second, the height of both the top and bottom layers is increased to 300 nm. This height is comparable to the decay length of the plasmon field in the direction normal to the waveguide (294 nm) so that these two changes secure that 77% of the energy of the LRSPP are located within the gain layers. The density of molecules is increased by a factor of 3. Finally, instead of a gold waveguide a silver one is used. The propagation properties computed for this modified structure are shown as dashed lines in Fig. 2. As observed in this figure, the above described changes make it possible to access values of the propagation constants of  $\text{Im}(k_x) \gtrsim -1.8 \cdot 10^5 \text{ m}^{-1}$ .

As an example of the typical dynamics of the lasing action, we study the time dependency of the amplitude of the LRSPP-mode ( $\omega_{SPP} = 2.98 \cdot 10^{15} \text{ s}^{-1}$ ) in a waveguide with  $|r| = 0.95$  and a length of  $l = 2\lambda_{SPP} = 724 \text{ nm}$ ,  $\lambda_{SPP}$  being the modal wavelength of the plasmon. Notice that the emission of the molecules and the plasmon mode are in resonance, in such a way that an optimal coupling of the plasmon to the gain medium is achieved. In these simulations, the system is optically pumped until the steady state of the population densities is reached. Once that steady-state has been achieved, the LRSPP mode is *switched on*. The time dependency of the LRSPP amplitude for pump intensities above the threshold ( $E_{th} \approx 4.9 \cdot 10^6 \text{ V/m}$ ) shows the characteristic lasing behavior (see Fig. 3). After displaying a series of spikes at lower values of time, the modal amplitude of the LRSPP reaches a steady-state (after around 0.6–0.7 ns, or equivalently  $3 \cdot 10^5$  optical periods). The inset shows how the intensity of the LRSPP mode in the steady state depends on the pump intensity. Above the threshold the characteristic linear dependency of lasing action is clearly observed. We have also performed control simulations without the metallic waveguide in order to highlight that the lasing action is assisted by long-range surface plasmons.

As our numerical framework includes the full spatial and temporal dynamics of both the electromagnetic field and the population densities of the molecular states, it enables us to study the microscopic origin of the lasing action and the details of the interplay between the field distribution and the population densities. In Fig. 4, the spatial distributions of the field and the population density of excited DCM molecules are shown. These results display how the feedback introduced by the reflective boundaries leads to the formation of a standing wave with a LRSPP-field profile within the waveguide. As seen in Fig. 4, the

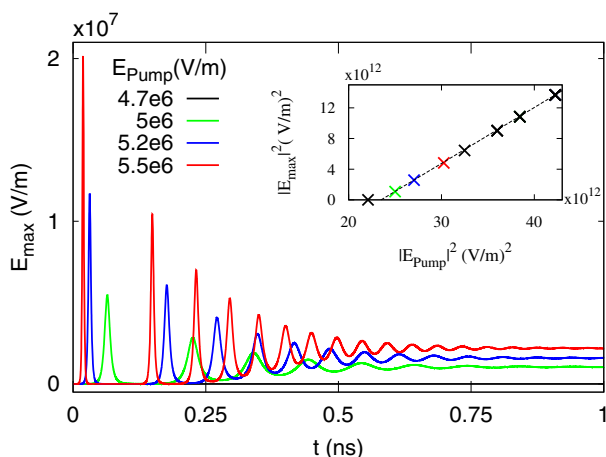


**Figure 3** Dynamics of the lasing action. The time dependency of the amplitude of the electric field (taken at a maximum within the waveguide) for different pumps is shown in the main plots. For pump intensities above the threshold ( $E_{th} \approx 4.9 \cdot 10^6 \text{ V/m}$ ) the typical lasing dynamics is found. The results are shown for a waveguide length of  $l = 2\lambda_{SPP} = 724 \text{ nm}$  and  $|r| = 0.95$ . The inset shows the linear dependency of the SPP intensity (averaged over the gain layers) in the steady state on the pump intensity.

LRSPP provides subwavelength confinement in the vertical direction (the corresponding decay length being 294 nm, which is smaller than  $\lambda/n = 370 \text{ nm}$ ). Note that the physical mechanism responsible for this vertical confinement is plasmonic in nature, and, therefore, it differs from the total internal reflection mechanism that characterizes high-index dielectric (non-plasmonic) waveguides. In addition, notice how the interplay between the plasmon field and the population density causes a non-uniform density of excited DCM molecules (see lower panel of Fig. 4). It is particularly apparent how the maxima in the field distribution induce minima in the singlet density. The displayed population density also illustrates again how the Purcell effect depends on the pump intensity. Given that the structure is pumped from above, the pump intensity above the waveguide is significantly higher than below. This in turn leads to a layer of quenched molecules below the waveguide much thicker than the one above the metal (as indicated by the blue layers below and above the waveguide in the lower panel of Fig. 4). To the best of our knowledge, this is the first time that such dependence of the Purcell effect on the electric field intensity has been reported in the context of lasing action at subwavelength scales.

In conclusion, we have analyzed the lasing behavior of long range surface plasmons using a novel numerical method that includes the full spatial and temporal dynamics of the electromagnetic field and of the gain medium. We have shown how the low propagation losses of LRSPP can lead to low lasing thresholds in systems than incorporate optical feedback. These low lasing thresholds, together with the planar and subwavelength character of LRSPP, make the structures analyzed in this work promising candidates for creating novel types of coherent light sources suitable

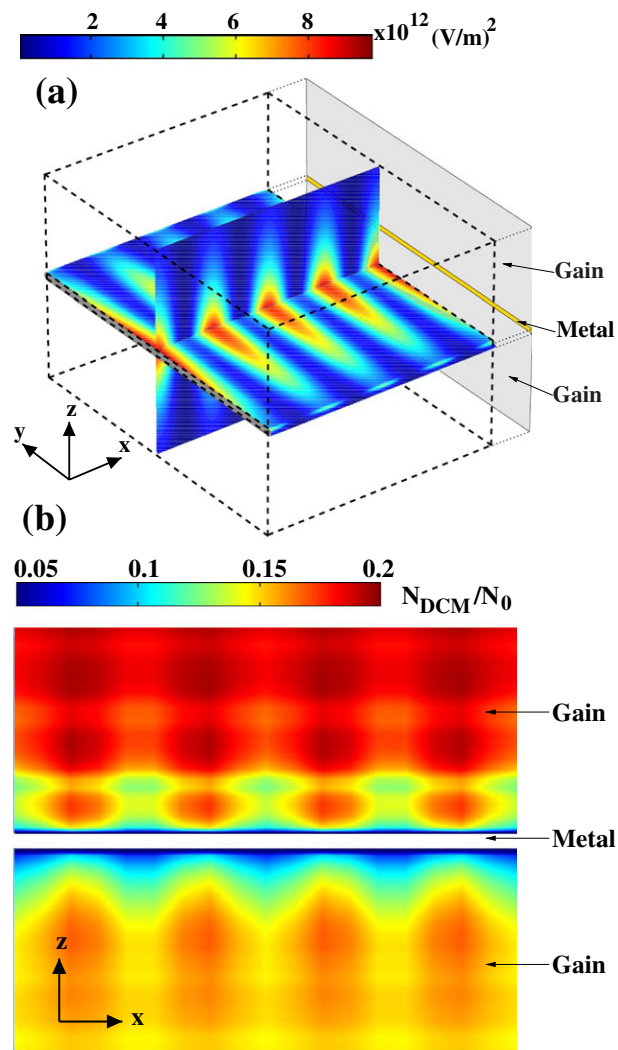


**Figure 4** Spatial distribution of the field intensity (a) and DCM singlet density (b) in the lasing regime. The top panel shows the intensity distribution of the LRSPP mode. The reflective boundaries lead to a standing wave within the waveguide. While the pump field is uniform along the propagation direction ( $x$ -direction), the interplay between the LRSPP-field and population density leads to a non-uniform singlet density (lower panel). The results are shown for a pump of  $E_{pump} = 5.5 \cdot 10^6 \text{ V/m}$  and the field intensity is presented in the steady state while the population is shown shortly after the first lasing spike.

for their integration in plasmonic circuits. Furthermore, we believe that the numerical method introduced in this work provide a powerful tool for analyzing, designing, and optimizing not only LRSPP subwavelength scale lasers, but also a broad variety of other subwavelength lasing devices.

**Acknowledgements.** This work has been funded by the European Research Council (ERC-2011-AdG Proposal No. 290981). The authors also acknowledge financial support from the Spanish MINECO project MAT2011-28581-C02-01.

**Supporting Information:** for this article is available free of charge under <http://dx.doi.org/10.1002/lpor.201400052>

**Received:** 8 March 2014, **Revised:** 22 May 2014,

**Accepted:** 3 June 2014

**Published online:** 1 July 2014

**Key words:** Plasmonic lasing, long-range surface plasmons, Purcell effect.

## References

- [1] P. Berini, *Adv. Opt. Photon.* **1**(3), 484–588 (2009).
- [2] R. Charbonneau, C. Scales, I. Breukelaar, S. Fafard, N. Lahoud, G. Mattiussi, and P. Berini, *J. Lightwave Technol.* **24**(1), 477–494 (2006).
- [3] A. Boltasseva, T. Nikolajsen, K. Leosson, K. Kjaer, M. S. Larsen, and S. I. Bozhevolnyi, *J. Lightwave Technol.* **23**(1), 413 (2005).
- [4] M. A. Noginov, G. Zhu, A. M. Belgrave, R. Bakker, V. M. Shalaev, E. E. Narimanov, S. Stout, E. Herz, T. Suteewong, and U. Wiesner, *Nature* **460**(7259), 1110–1112 (2009).
- [5] J. Y. Suh, C. H. Kim, W. Zhou, M. D. Huntington, D. T. Co, M. R. Wasielewski, and T. W. Odom, *Nano Letters* **12**(11), 5769–5774 (2012).
- [6] Y. J. Lu, J. Kim, H. Y. Chen, C. Wu, N. Dabidian, C. E. Sanders, C. Y. Wang, M. Y. Lu, B. H. Li, X. Qiu, W. H. Chang, L. J. Chen, G. Shvets, C. K. Shih, and S. Gwo, *Science* **337**(6093), 450–453 (2012).
- [7] W. Zhou, M. Dridi, J. Y. Suh, C. H. Kim, D. T. Co, M. R. Wasielewski, G. C. Schatz, and T. W. Odom, *Nat. Nano.* **8**(7), 506–511 (2013).
- [8] F. van Beijnum, P. J. van Veldhoven, E. J. Geluk, M. J. A. de Dood, G. W. 't Hooft, and M. P. van Exter, *Phys. Rev. Lett.* **110**(May), 206802 (2013).
- [9] R. M. Ma, R. F. Oulton, V. J. Sorger, and X. Zhang, *Laser & Photonics Reviews* **7**(1), 1–21 (2013).
- [10] R. F. Oulton, V. J. Sorger, T. Zentgraf, R. M. Ma, C. Gladden, L. Dai, G. Bartal, and X. Zhang, *Nature* **461**(7264), 629–632 (2009).
- [11] S. H. Kwon, J. H. Kang, C. Seassal, S. K. Kim, P. Regreny, Y. H. Lee, C. M. Lieber, and H. G. Park, *Nano Letters* **10**(9), 3679–3683 (2010).
- [12] R. M. Ma, R. F. Oulton, V. J. Sorger, G. Bartal, and X. Zhang, *Nat. Mater.* **10**(2), 110–113 (2011).
- [13] K. Tsakmakidis and O. Hess, Slow and stopped-light lasing in active plasmonic metamaterials, in: *Transparent Optical Networks (ICTON)*, 14th International Conference (2012), pp. 1–6.
- [14] S. Kéna-Cohen, P. N. Stavrinou, D. D. C. Bradley, and S. A. Maier, *Nano Letters* **13**(3), 1323–1329 (2013).
- [15] I. De Leon and P. Berini, *Nat. Photon.* **4**(6), 382–387 (2010).
- [16] A. Boltasseva, S. I. Bozhevolnyi, T. Nikolajsen, and K. Leosson, *J. Lightwave Technol.* **24**(2), 912 (2006).
- [17] C. Fietz and C. M. Soukoulis, *Opt. Express* **20**(10), 11548–11560 (2012).
- [18] J. M. Hamm, S. Wuestner, K. L. Tsakmakidis, and O. Hess, *Phys. Rev. Lett.* **107**(Oct), 167405 (2011).
- [19] A. Pusch, S. Wuestner, J. M. Hamm, K. L. Tsakmakidis, and O. Hess, *ACS Nano* **6**(3), 2420–2431 (2012).
- [20] M. Dridi and G. C. Schatz, *J. Opt. Soc. Am. B* **30**(11), 2791–2797 (2013).
- [21] J. Jin, *The Finite Element Method in Electromagnetics* (Wiley, New York, 2002).